Analysis of Multiple Scattering Characteristics of Cable-Stayed Bridges with Multi-band SAR

Yanhao Xu[1], Yangmao Wen[1], Tao Li[2], Sijie Ma[2], Jie Liu[2]

[1] School of Geodesy and Geomatics, Wuhan University, Wuhan,430079, China;
[2] Research Center of GNSS, Wuhan University, Wuhan, 430079,China;

Keywords: SAR, Cable-Stayed Bridge, Multiple Scattering, Multi-band, Range-Doppler,Water Level

Abstract

Accurate localization of multi-scattering features of cable-stayed bridges in multi-band Synthetic Aperture Radar (SAR) imagery is crucial for intelligent recognition of bridge targets within images, as well as for precise water level extraction. This study focuses on the Badong Yangtze River Bridge, utilizing Unmanned Aerial Vehicle (UAV) LiDAR data of the bridge, and analyzes the multi-scattering characteristics of different bridge structural targets based on Geometric Optics (GO) methods and the Range-Doppler principle. Furthermore, the study integrates LiDAR data of the bridge's cable-stays to examine their multi-scattering phenomena, finding that the undulations of the Yangtze River's surface waves significantly contribute to the pronounced double scattering features of the bridge's cable-stays. Additionally, statistical analysis of multi-source SAR data indicates that this phenomenon is not directly correlated with radar wavelength, implying no direct connection to surface roughness. Utilizing LiDAR point cloud data from the bridge's street lamps, this paper proposes a novel method for estimating water level elevation by identifying the center position of spots formed by double scattering from lamp posts. The results show that using TerraSAR ascending and descending orbit images, this method achieves a water level elevation accuracy of approximately 0.2 meters.

1. Introduction

Bridges, as indispensable man-made structures in transportation, have their status and safety as critical observational indicators for bridge monitoring(W.Zhao et al. 2006). Synthetic Aperture Radar (SAR), with its all-weather capability, has become a vital tool in bridge research. Bridge structures are complex, and the scattering of SAR signals at various structural points creates multiple bright lines in images(Ying,W et al. 1995). Wegner et al. (Wegner et al. 2008) compared differences between aquatic and terrestrial bridges, noting that double and third scattering caused by interactions between the bridge and land are usually undetectable in SAR images. Lee et al. simulated the multi-scattering phenomena of large cable-stayed bridges using polarized SAR data and point scatter models(Lee et al. 2006). Additionally, bridge water surface heights can be inverted using airborne polarized SAR data. Wang et al. simulated aquatic bridges in SAR images using a mapping projection algorithm and successfully located them in the images through the Hough transform. Bridge multi-scattering features are related to multipath scattering mechanisms (Wang et al. 2009), and high-resolution imagery enables more detailed observations, facilitating the inversion of bridge parameters (Cadario et al. 2008;Zhang, Y., et al 2015). Gan et al. studied the imaging characteristics of non-linear bridges, focusing on the effects of azimuth and surface roughness(Gan et al. 2017). With the increasing launch of high-resolution SAR satellites, extracting multi-scattering lines from SAR images using theHough transform to estimate water level changes has become routine(Chen et al. 2021; Kim et al. 2022). Although previous studies primarily focused on the images rather than the actual structure of the bridge, knowing the exact geographical coordinates of a bridge allows one to accurately determine its position in SAR images through the Range-Doppler (R-D) model(Wang 2017; Wen 2020;Song et al. 2021). This paper, utilizing LiDAR point cloud data from the Badong Yangtze River Bridge, proposes a simulation method for bridge multi-scattering features based on bridge LiDAR data and the R-D model. It also introduces a novel method to estimate river water levels using double scattering from lamp posts on the bridge in high-resolution SAR images, which has been experimentally validated in the Badong Yangtze River Bridge area.

2. Study area and data sources

The research area, Badong Yangtze River Bridge, is located in the Three Gorges Reservoir area of the middle Yangtze River in Badong County, Hubei Province, China. The bridge consists of the main bridge, two bridge towers, cable-stays, piers, and bridge deck infrastructure. The main bridge section is oriented from northwest to southeast, with a total length of 900.6 meters and a main span of 388 meters, forming an angle of 20.6 degrees with true north.

Figure 1. Photos of Badong Yangtze River Bridge

Figure 2 displays the satellite imagery of the Badong Yangtze River Bridge. (a) shows the optical image of the bridge, while (b) and (c) are the SAR satellite images from ascending and descending orbits, respectively. Comparing the optical and SAR images reveals noticeable differences in the bridge's representation. In the SAR images, the bridge imaging can be roughly divided into three parts, each caused by scattering from different bridge structures.

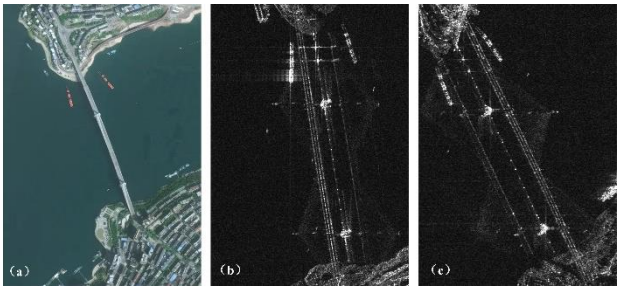

Figure 2.Satellite remote sensing image of Badong Yangtze River Bridge

This article collects multi-source SAR data in the Badong Yangtze River Bridge area from 2017 to 2021. The detailed data information is shown in Table 1.

Table 1
Basic parameters of multi-source SAR

Satellite	Orbit	Band	Incidence Angle	Range pixel spacing	Heading	Number
TerraSAR-X	ASC	X	38.1°	0.91m	-11.8°	54
	DES	X	28.7°	0.91m	191.8°	48
COSMO-Skymed	ASC	X	20.1°	0.77m	-12.4°	2
	DES	X	26.6°	0.92m	192.4°	2
Radarsat-2	ASC	C	30.3°	1.33m	-13.3°	8
	DES	C	34.6°	1.33m	193.3°	7
ALOS-2	ASC	L	33.0°	1.43m	-12.4°	22
	ASC	L	43.7°	1.43m	-12.4°	7

3. Methodology

The SAR satellite orbits have different ascending and descending flight directions, none of which align with the orientation of the Badong Yangtze River Bridge. There is an angular deviation between the radar line of sight and the direction of the bridge. As shown in Figure 3, the conversion relationship between the distance in pixels (N) of the bridge deck scattering lines in the SAR images and the actual spacing (L) of the bridge railings is as follows:

$$\theta_a = \psi_1 - \psi \quad (1)$$

$$\theta_d = \psi_1 + \psi - 180^\circ \quad (2)$$

$$Ls_a = L/\cos\,\theta_a \quad (3)$$

$$Ls_d = L/\cos\,\theta_d \quad (4)$$

$$N = Ls * sin\eta/\mathrm{R} \quad (5)$$

where θ_a, θ_d= the angles between the radar line of sight and the bridge direction for the ascending and descending orbits

ψ = the angle between the SAR satellite's flight direction and the north

ψ_1= the angle between the bridge direction and the north

L= the actual spacing between the bridge railings

Ls_a, Ls_d =the radar line of sight distances between the bridge railings under ascending and descending orbits

N = the difference in distance-oriented pixels of the bridge deck scattering lines in the SAR images

η = the incidence angle of the SAR satellite

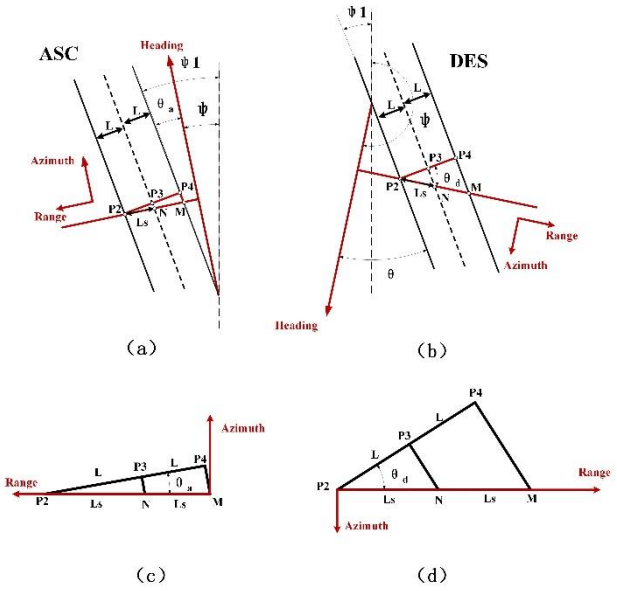

Figure 3 The relationship between the flight direction of the SAR satellite and the direction of the bridge, in which (a) is the ascending orbit, (b) is the descending orbit, (c) and (d) are the ascending/descending radar line of sight triangles respectively.

In this section, we will introduce the combination of bridge LiDAR point cloud data and Range-Doppler frequency shift to simulate the multi-scattering phenomena of bridges and the use of SAR images to measure river water levels through geometric models and mathematical expressions. If the direction of the bridge is not perpendicular to the satellite orbit, three bright parallel stripes will appear in high-resolution SAR images, representing: bridge deck scattering, double scattering between the bridge and the water surface, and third scattering involving the water surface, bridge, and water surface again. This phenomenon is due to the relative positions of the bridge, satellite, and water level, the reflection and refraction of microwaves, and the geometric configuration captured by synthetic aperture radar.

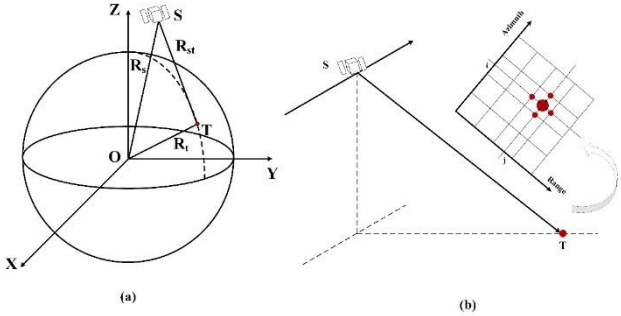

Figure 4 SAR satellite and ground point R-D schematic diagram

The Range-Doppler model is based on the imaging mechanism of SAR imagery, utilizing the sensor-target distance, echo signal Doppler, and the Earth's ellipsoid equation to establish a precise geometric relationship between the image pixel coordinates and the ground target points.

As shown in Figure 4(a), S represents the SAR satellite, and T is the target point on the Earth's surface. The distance $\mathbf{R}_{st}$ determined by the instantaneous position of the SAR sensor and the target can be represented as:

$$\mathbf{R}_{st} = |\mathbf{R}_s - \mathbf{R}_t| = \sqrt{(X_S - X_T)^2 + (Y_S - Y_T)^2 + (Z_S - Z_T)^2} \quad (6)$$

where $\mathbf{R}_s = (X_S Y_S, Z_S)^T$ is the position vector of the SAR satellite

$\mathbf{R}_t = (X_T, Y_T, Z_T)^T$ is the position vector of target point T

As the radar beam passes the target, there is relative motion between the SAR sensor position S and the ground target T. Due

to the Doppler effect, the frequency of the radar echo signal shifts, and the Doppler shift is given by:

$$f_D = -\frac{2}{\lambda}\frac{dR}{dt} = -\frac{2}{\lambda}\frac{(\mathbf{R}_s - \mathbf{R}_t)(\mathbf{V}_s - \mathbf{V}_t)}{|\mathbf{R}_s - \mathbf{R}_t|} \quad (7)$$

where λ= the radar wavelength

f_D= the Doppler center frequency for that point

$\mathbf{R}_t, \mathbf{V}_t$= the position vector and velocity vector of point T

$\mathbf{R}_s, \mathbf{V}_s$ =the position vector and velocity vector of the satellite at the imaging moment of point T

Using LiDAR data, geographical coordinates (λ, ϕ, h) of the bridge target point T can be obtained. Starting from the geographical coordinates of the target point, using known satellite orbit parameters combined with the R-D model, the corresponding image plane coordinates (i, j) can be calculated, where i and j refer to the azimuth and range indices of point target T in the SAR image, respectively. The specific calculation process is as follows:

(1)With the known WGS84 geographical coordinates (λ, ϕ, h) of ground target point T, its position vector $\mathbf{R}_t$ can be obtained through coordinate transformation as $(X_T, Y_T, Z_T)^T$;

(2) Set the azimuth coordinate i_c of the image center point under the radar coordinate system as the initial value of the image plane coordinate of ground target T, and calculate its corresponding azimuth time t_i;

$$t_i = t_{az} + \frac{i_c - 1}{PRF} \quad (8)$$

where t_{az}= the start time of the first line of the SAR image

i_c= the azimuth coordinate of the image center point

PRF= the pulse repetition frequency

(3) Based on the azimuth time t_i, interpolate to calculate the sensor's position vector $\mathbf{R}_s$ and velocity vector $\mathbf{V}_s$;

(4) Substitute the sensor's position $\mathbf{R}_s$ and velocity $\mathbf{V}_s$ as well as the ground target point coordinates $\mathbf{R}_t$ into Equation (7) to calculate the Doppler frequency value f_D, and simultaneously calculate the Doppler frequency reference value f_d based on the azimuth time, solving for the change in azimuth time d_t :

$$d_t = \frac{f_D - f_d}{f_d'} \quad (9)$$

where f_d' = the rate of change of Doppler frequency, which is the derivative of f_D with respect to time t_i ;

(5) Recalculate the azimuth time $t_i = t_{i-1} + d_t$, check if d_t satisfies the set error threshold; if it does, output the image plane row number i; otherwise, repeat steps (3)-(5) until the requirement is met.

(6) Using Equation (6), calculate the slant distance from the SAR sensor position to the ground target point, thereby obtaining its image plane column number j.

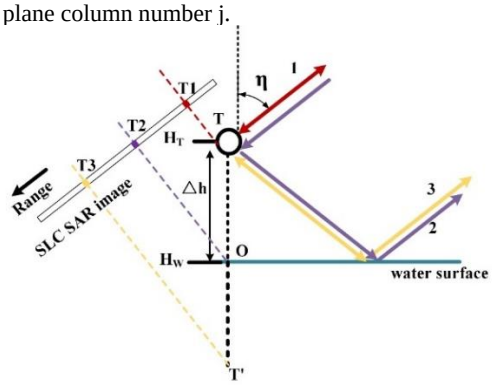

Figure 5 Multiple scattering model of bridge structure based on R-D

Assuming the presence of multi-scattering phenomena at a certain point on the bridge, the geometric principles of such multi-scattering are illustrated in Figure 5. LiDAR can determine the geographical coordinates (latitude λ, longitude ϕ, height h) of the target point T, with the multi-scattering points T1, T2, T3 in the SAR image representing the image pixel coordinates of points T, O, and T' in the SAR image. Points T, O, and T' share the same latitude λ and longitude ϕ, which can be acquired through LiDAR data, differing only in elevation. O is the vertical projection of point T onto the water surface, and points T and T' are symmetrical about point O. Using the previously described R-D model, the row and column numbers in the SAR image can be obtained from the latitude, longitude, and altitude coordinates of the target point. Thus, the SAR image row and column numbers (i, j) for point T1 can be obtained from the geographical coordinates (latitude λ, longitude ϕ, height h) of point T, allowing for the simulation and validation of the bridge's multi-scattering features combined with LiDAR data.

4. Result

4.1. Analysis of Scattering Characteristics of Badong Bridge Deck

Selecting the highest resolution TerraSAR data from multi-source SAR satellite imagery, an average intensity image was produced as shown in Figure 6(a). The scattering characteristics of the bridge in the image are exceedingly complex, with distinct differences in bridge features under ascending and descending orbit conditions. The consistent scattering texture between the orbits presents three bright lines on the bridge deck, which are likely related to the scattering features formed by five rows of symmetrically distributed railings on the bridge surface.

Based on 3D point cloud data from LiDAR scanning, it is known that there are five rows of railings distributed on the deck of the Badong Yangtze River Bridge. These are numbered P1-P5 from west to east. The central railing, approximately 0.6m in height, is used to separate the vehicular lanes; the railing on the riverside of the pedestrian pathway is about 1.1m high, ensuring the safety of pedestrians; the railing closest to the vehicular lane on the pedestrian pathway is approximately 0.4m high. As the pedestrian walkways are symmetrically arranged on the bridge deck, the railings on both sides are also symmetrically distributed. LiDAR point cloud data collected on-site indicates that the bridge deck is 22 meters wide, with the spacing of the railings on either side of the pedestrian pathways being 1.5m (L12, L45), and the spacing between the pedestrian and vehicular lane separating railings being 8m (L23; L43).

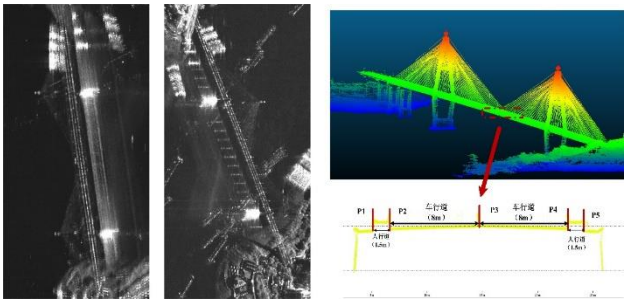

Figure 6 Average intensity map and LiDAR bridge deck structure

Considering the dihedral corner reflector theory, the bridge railings along with the concrete and asphalt surfaces on the bridge deck create a dihedral corner reflector, which enhances the backscatter signal(Ferretti et al. 2007). By precisely locating the dihedral scattering centers of the 5 railings in both ascending and descending track modes, the accuracy of this theoretical method can be verified. The LiDAR point cloud data for railings P1-P5 are extracted, and based on the R-D positioning model, their latitude and longitude coordinates are converted to SAR coordinates and superimposed onto the SAR image layer. The results, as shown in Figure 6, indicate that the bridge deck scattering is caused by the dihedral corners formed by the deck and railings. Due to the short distance L12 (L45) of only 1.5m, they form a single scattering line in the SAR image, hence only three bridge deck scattering lines are observed.

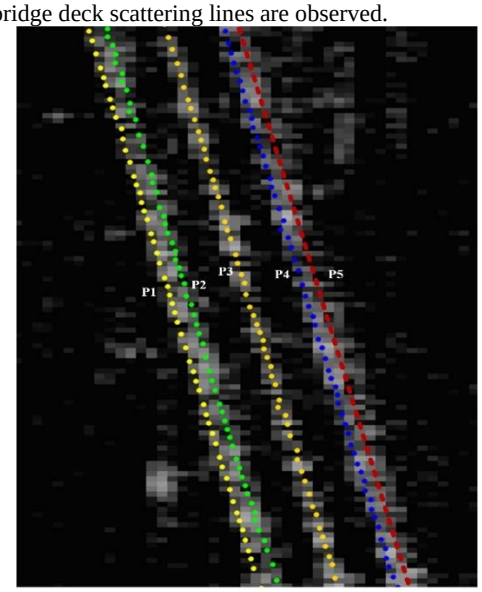

Figure 7 Badong Yangtze River Bridge deck scattering simulation diagram

The Hough Transform is used to extract the scattering lines on the bridge deck and to estimate the range-oriented pixel difference Ne between railing P3 and railings P2/P4 in the SAR image. Using the bridge deck LiDAR and equations (5)-(9), the multi-source SAR data in Table 1 is processed to calculate the theoretical range-oriented pixel difference N between railing P3 and railings P2/P4 in the SAR image, as shown in Table 2.

Table 2

Satellite	Orbit	Pixel difference N in the distance direction between railing P3 and P2/P4 in the SAR image	Estimated pixel difference Ne in the distance direction between railing P3 and P2/P4 in the SAR image
TerraSAR-X	ASC	5.00	4.89
	DES	4.55	4.68
COSMO-Skymed	ASC	2.78	2.59
	DES	4.27	4.12
Radarsat-2	ASC	4.07	4.23
	DES	5.47	5.71
ALOS-2	ASC	4.40	4.52
	DES	5.58	5.70

4.2. Analysis of multiple scattering characteristics of stay cables

Compared to the Great Belt Bridge studied by Jong-Sen Lee, the diameter of the stay cables of the Badong Yangtze River Bridge is only 0.2m, which is significantly smaller than the main cable diameter of the Great Belt Bridge. By combining on-site LiDAR point cloud data, the point clouds of the stay cables of the Badong Yangtze River Bridge were filtered to extract their geographic coordinates (latitude and longitude) and elevation (h) under the WGS84 coordinate system. Using the R-D positioning model, the pixel positions in the SAR images were obtained. Water level data from the dates when the SAR images were captured were collected, and combined with formulas (6) to (9) and the latitude, longitude, and elevation data of the stay cables, as well as the water level elevations, to simulate the multiple scattering characteristics of the Badong Yangtze River Bridge stay cables. The results are shown in Figure 8, which indicates that the simulated results are consistent with the actual multiple scattering imaging of the stay cables in the SAR images.

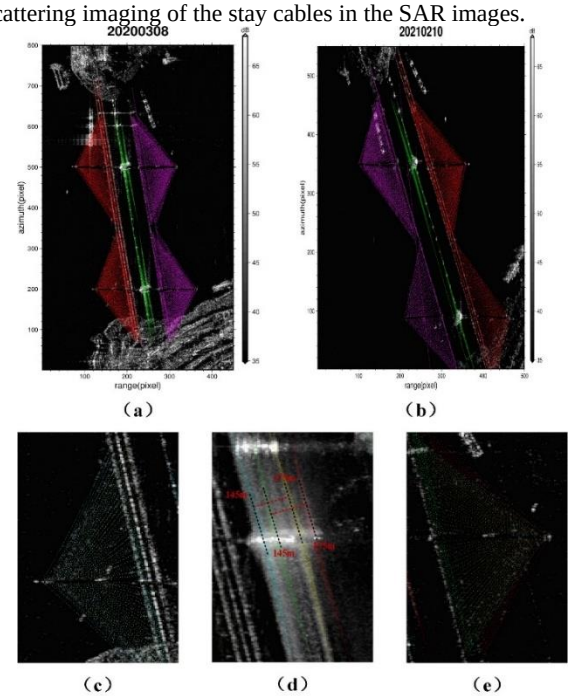

Figure 8. Simulation diagram of multiple scattering of the cable-stayed cables. Among them (a) (b) are the simulation diagrams of multiple scattering of the stay cable under the lifting track respectively, (c) (d) (e) are the primary scattering, second scattering and third scattering of the stay cable under the lifting track respectively. Scattering simulation

Figure 8 shows the imaging of the Badong Yangtze River Bridge in multi-source SAR images. Panels (a), (b), and (c) display TerraSAR-X images, where variations in the multiple scattering imaging of the stay cables can be observed, including weak double scattering signals, strong signals, and signal expansion. In panels (d) and (e) with C-band Radarsat-2 ascending and descending track images, and (f) with L-band

ALOS-2 ascending track images, it is difficult to discern the primary and third scattering features of the stay cables. However, the double scattering features of the stay cables are still observable in the majority of the images.

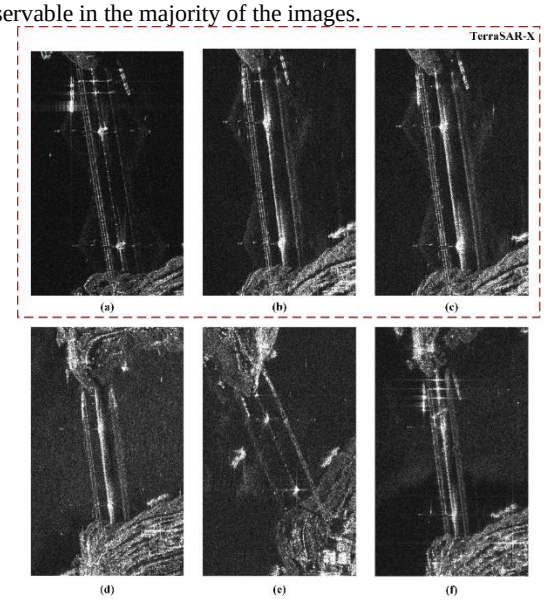

Figure 9 Multiple scattering characteristics of stay cables in multi-source SAR

According to the aforementioned classification standards for TerraSAR-X images, the results are as follows:

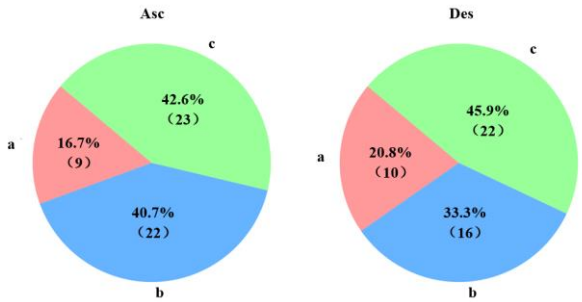

Figure 10 Category Pie Chart

In high-resolution TerraSAR-X images, the double scattering of the stay cables on both sides of the Badong Yangtze River Bridge is clearly observable, indicating that the stay cables on both sides participate in primary, double, and third scattering characteristics, all capable of producing reflective signals, with internal diffraction phenomena within the stay cable structure not being prominent. Theoretically, the double scattering of the stay cables does not overlap and is relatively independently distributed, with the imaging location concentrated and the signal stronger compared to primary and third scatterings. The primary scattering features of the stay cables overlap with the bridge surface scattering line signals, presenting an overlay effect; similarly, the third scattering lines overlap with the bridge's third scattering line signals.

There are variations in the multiple scattering features of the stay cables in multi-source SAR images, which are due to differences in image resolution. Only the TerraSAR-X images with better than 1m resolution can clearly distinguish the multiple scattering phenomena of the stay cables. The Radarsat-2 and ALOS-2 images are affected by resolution, and due to the dispersion of primary and third scattering signals of the stay cables, they cannot be recognized in low-resolution images. In contrast, the double scattering signals are independently distributed and relatively concentrated. In complex hydrological scenes like the Yangtze River with significant water surface fluctuations, the fluctuations actually make the double scattering features easier to identify, and resolution differences do not significantly impact the double scattering of the stay cables. Thus, in images with lower resolutions, only the double scattering phenomena of the stay cables can be seen. Therefore, the prominent double scattering features of the stay cables significantly aid in the intelligent recognition and automatic interpretation of the corresponding stay cable bridges in SAR images.

4.3. Target water level estimation by double scattering points

As shown in Figure 11, by selecting parts of the TerraSAR data where the double scattering phenomenon of the stay cables is weak to create an average intensity image, multiple bright spots can be observed along the bridge's double scattering line. These are estimated to be the imaging of double scattering from the bridge's lampposts and the water surface. The bridge lampposts are cylindrical and thus have strong scattering characteristics for radar waves coming from different incident directions. By combining the R-D model with on-site LiDAR geographical coordinates, and simulating the multiple scattering characteristics of the stay cables, the double scattering of the lampposts is simulated to confirm that the bright spots are indeed the double scattering from the lampposts. In the Badong region, the Yangtze River water level fluctuates annually between 145m and 175m, and corresponding positional changes can also be observed in the double scattering from the lamppost points in Figure 11.

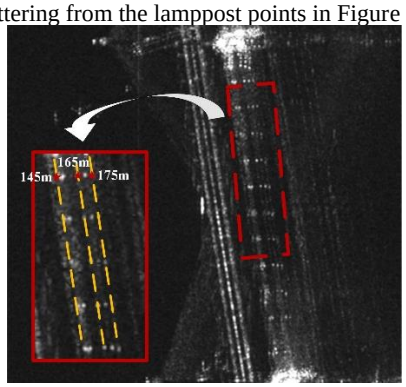

Figure 11 double scattering simulation of street lamps

Using the R-D model, the latitude and longitude coordinates of each lamppost can be obtained through LiDAR, and by combining equations (6) to (9), the fluctuations of the streetlights with the water surface can be individually simulated. Conversely, by identifying the center position of the double scattering of the lampposts in each SAR image, the water level height can be estimated. The imaging position of each lamppost in the SAR images at different water levels is simulated, with the water level in the Three Gorges Reservoir area fluctuating from 145m to 175m, simulating the double scattering imaging position of the lampposts at every 0.1m interval between 145m and 175m. By checking the closest distance between the simulated points and the actual center position of the lamppost’s double scattering in the SAR images, the water level height under the bridge at the time of image capture can be estimated. The clarity of the double scattering imaging of the lampposts is affected by water surface fluctuations; when the water fluctuation is significant, the double scattering imaging of the stay cables can cover the lampposts’ double scattering, making it impossible to estimate the water level in such cases.

According to Figure 10, in 102 TerraSAR images, only 19 images clearly identify the double scattering phenomenon of the lampposts. The water level values for these 19 images are calculated, with results shown in Table 3.

Table 3 water level estimation

Date	Orbit	$H_{water}^{estimated}$ (m)	$H_{water}^{measured}$ (m)	Difference between estimated and measured water level (m)
Dec 11, 2019	ASC	174.6	174.47	0.13
Jan 24, 2020	ASC	169.8	169.78	0.02
Mar 08, 2020	ASC	167.1	167.00	0.1
May 02, 2020	ASC	157.1	157.28	-0.18
May 13, 2020	ASC	153.4	153.28	0.12
Jul 07, 2020	ASC	148.9	148.87	0.03
Jan 21, 2021	ASC	170.2	170.1	0.1
Feb 12, 2021	ASC	169.4	169.2	0.2
Feb 23, 2021	ASC	167.3	167.29	0.01
Feb 13,2020	DES	167.3	167.48	-0.18
Jun 24, 2020	DES	146.8	146.69	0.11
Jul 27, 2020	DES	160.4	160.56	-0.16
Feb 10, 2021	DES	169.3	169.54	-0.24
Feb 21, 2021	DES	167.4	167.66	-0.26
Mar 04, 2021	DES	166.4	166.45	-0.05
Mar 26, 2021	DES	165.7	165.87	-0.17
May 20, 2021	DES	153.4	153.3	0.1
Jun 11, 2021	DES	145.4	145.32	0.08
Sep 07, 2021	DES	164.9	164.8	0.1

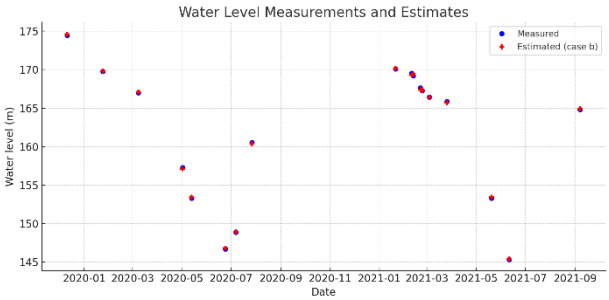

Figure 12 Estimated water level from SAR acquisitions.

5. Discussion and Conclusion

By integrating LiDAR data with the R-D model, it is possible to accurately calculate the imaging positions of various bridge structures on radar. Simulations of dihedral angle scattering from the bridge's railing surface confirm the involvement of five railings in the formation of three bridge surface scattering lines. Considering differences in satellite orbit direction and incidence angle, calculations of the spacing between bridge surface scattering lines under multiple-source SAR ascending and descending orbits yield theoretical values. The Hough transform is used to extract bridge surface scattering lines and estimate the spacing between them. TerraSAR data achieves the highest precision, with a discrepancy of about 0.1 pixels; discrepancies in other data are about 0.2 pixels.

In the dataset of 102 TerraSAR images, less than 20% show weak double scattering from stay cables. Most of the images indicate that water surface waves significantly affect both double scatterings of the stay cables. In over 40% of the images, water surface waves cause an expansion of the double scattering features of the stay cables, making them very prominent and easy to identify. Therefore, in the Yangtze River Three Gorges Reservoir area, the double scattering phenomenon of stay cables can effectively help in identifying cable-stayed bridges on the water surface.

In the Badong Yangtze River Bridge area, if the geographic coordinates of the bridge's lamp posts are known, the R-D model can be used to estimate the water level. Taking TerraSAR data as an example, the estimated results are fairly consistent with the measured absolute water levels, with an estimation accuracy of about 0.2 meters in ascending and descending orbit images. The accuracy of the water level estimation is better than 20% of the image's spatial resolution, which fits within the acceptable error range. However, only less than 20% of the total number of images are suitable for using this method to estimate water levels, indicating significant limitations of this estimation method in hydrologically complex and dynamically fluctuating environments like the Yangtze River, and not all SAR images are capable of accurate calculations.

By combining LiDAR data, the methods described in this paper can be applied to simulate bridges over water surfaces. Additionally, the water level can be estimated through the double scattering phenomena of specific target points on the bridge surface.

References

W. Zhao, J. Song and J. Zhang, "Study on the detection algorithm of bridge over water in SAR image based on fuzzy theory", The First International Conference on Innovative Computing Information and Control (ICICIC), vol. 3, pp. 641-644, 2006.

Ying, W. and Z. Qinfen. Recognition of roads and bridges in SAR images. in Proceedings International Radar Conference. 1995.

Wegner, J.D. and U. Soergel. Bridge height estimation from combined high-resolution optical and sar imagery. 2008. Beijing, China: International Society for Photogrammetry and Remote Sensing.

Lee, J., et al., Polarimetric analysis of radar signature of a manmade structure. Asia-Pacific Microwave Conference Proceedings, APMC, 2006.

WANG Hai-peng, X.F.J.Y., Estimation of the bridge height over water using SAR image data. Journal of Remote Sensing, 2009. 13(03): p. 385-390.

Zhang, Y., et al., The Characteristics of the Multipath Scattering and the Application for Geometry Extraction in High-Resolution SAR Images. IEEE Transactions on Geoscience and Remote Sensing, 2015. Issue 8(Volume 53): p. Pages 4687-4699.

Cadario E , Schulz K , Gross H , et al. Feature extraction and change detection for bridges over water in airborne and spaceborne SAR image data. 2008.

Gan, X., et al. Influence of azimuth angle and water surface roughness on sar imagery of a bridge. in 2017 IEEE International Geoscience and Remote Sensing Symposium (IGARSS). 2017. Fort Worth, TX, United states: Institute of Electrical and Electronics Engineers Inc.

Chen, X., et al., Monitoring river water level using multiple bounces of bridges in SAR images. Advances in Space Research, 2021.

Kim, S.W. and Y.K. Lee, Accurate Water Level Measurement in the Bridge Using X-Band SAR. IEEE Geoscience and Remote Sensing Letters, 2022.

Wang Yachao. Research on Key Techniques of Stereo Matching for Stereo-Radargrammetry [D]. China University of Mining and Technology,2017.

Wen Yinkan. Optimization of Corner Reflector and Its Application in Spaceborne SAR image[D].Wuhan University,2020.

SONG Ruiqing, et al.Absolute Geolocation of Corner ReflectorsUsing High-Resolution Synthetic Aperture Radar images[J]. Journal of tongji university (natural science),2021,49(08):1202-1210.

Ferretti A, Savio G, Barzaghi R, Borghi A, Musazzi S, Novali F, Prati C, Rocca F. Submillimeter Accuracy of InSAR Time Series: Experimental Validation[J]. IEEE transactions on geoscience and remote sensing. 2007, 45(5): 1142-1153.